Available online at www.sciencedirect.com
SCIENCE DIRECT®
Journal of Solid State Chemistry 176 (2003) 111–119
JOURNAL OF SOLID STATE CHEMISTRY
http://elsevier.com/locate/jssc

Synthesis, structure, and molecular modeling of a titanoniobate isopolyanion

May Nyman,[a,*] Louise J. Criscenti,[a] François Bonhomme,[a] Mark A. Rodriguez,[b] and Randall T. Cygan[a]

[a] *Sandia National Laboratories, Geochemistry Department, Albuquerque, NM 87185-0750, USA*
[b] *Sandia National Laboratories, Materials Characterization Department, Albuquerque, NM 87185-0750, USA*

Received 27 February 2003; received in revised form 13 June 2003; accepted 28 June 2003

Abstract

Polyoxoniobate chemistry, both in the solid state and in solution is dominated by $[Nb_6O_{19}]^{8-}$, the Lindquist ion. Recently, we have expanded this chemistry through use of hydrothermal synthesis. The current publication illustrates how use of heteroatoms is another means of diversifying polyoxoniobate chemistry. Here we report the synthesis of $Na_8[Nb_8Ti_2O_{28}]\cdot 34H_2O$ [1] and its structural characterization from single-crystal X-ray data. This salt crystallizes in the *P*-1 space group ($a = 11.829(4)$ Å, $b = 12.205(4)$ Å, $c = 12.532(4)$ Å, $\alpha = 97.666(5)°$, $\beta = 113.840(4)°$, $\gamma = 110.809(4)°$), and the decameric anionic cluster $[Nb_8Ti_2O_{28}]^{8-}$ has the same cluster geometry as the previously reported $[Nb_{10}O_{28}]^{6-}$ and $[V_{10}O_{28}]^{6-}$. Molecular modeling studies of $[Nb_{10}O_{28}]^{6-}$ and all possible isomers of $[Nb_8Ti_2O_{28}]^{8-}$ suggest that this cluster geometry is stabilized by incorporating the Ti^{4+} into cluster positions in which edge-sharing is maximized. In this manner, the overall repulsion between edge-sharing octahedra within the cluster is minimized, as Ti^{4+} is both slightly smaller and of lower charge than Nb^{5+}. Synthetic studies also show that while the $[Nb_{10}O_{28}]^{6-}$ cluster is difficult to obtain, the $[Nb_8Ti_2O_{28}]^{8-}$ cluster can be synthesized reproducibly and is stable in neutral to basic solutions, as well.
Published by Elsevier Inc.

1. Introduction

In solid-state oxides containing titanium (Ti^{IV}) and niobium (Nb^{V}), these Periodic-table diagonal neighbors are often completely disordered over octahedral framework sites. This arises from the fact that both Ti^{IV} and Nb^{V} favor octahedral coordination and have similar ionic radii. The Ti^{IV}/Nb^{V} disorder in oxides has been observed in both natural systems and as products of laboratory solid-state or hydrothermal syntheses. Many minerals bearing disordered Ti^{IV}/Nb^{V} octahedral sites have been found in the Kola Peninsula in Russia [1–5]. Synthetic oxides containing disordered Ti^{IV}/Nb^{V} include layered perovskites such as the Dion–Jacobson and Ruddlesen–Popper phases [6–16], and microporous phases such as crystalline silicotitanate (CST) [17] and Sandia Octahedral Molecular Sieves (SOMS) [18,19].

More recent powder X-ray diffraction studies of layered perovskite materials have revealed that in perovskite-like slabs consisting of multiple layers of $Ti^{IV}/Nb^{V}O_6$ octahedra, the $Ti^{IV}O_6$ octahedra are concentrated in the interior layers while the $Nb^{V}O_6$ octahedra are concentrated in the exterior layers [20–23]. Prior to these studies, Gopalakrishnan et al. [24] also inferred this type of ordering of $Ti^{IV}/Nb^{V}O_6$ octahedra by comparing the Brønsted acidity of a mixed Ti^{IV}/Nb^{V} layered perovskite with that of the Nb^{V} end-member. The partial ordering of $Nb^{V}O_6$ octahedra in exterior slab sites and $Ti^{IV}O_6$ octahedra in interior slab sites has been attributed to several phenomenon including: (1) Nb^{V} (radius = 0.64 Å) associates with more distorted exterior sites than Ti^{IV} (radius = 0.60 Å) as a result of size and charge differences, to achieve maximum electronic stability [25]. (2) Local charge neutrality is achieved with interior $SrTiO_3$ subunits, and excess positive charge of Nb^{V} is compensated by the excess negative charge of the terminal (unshared) oxygen atoms in the inter-slab space [20,21]. (3) In the

*Corresponding author. Fax: +505-844-7354.
E-mail address: mdnyman@sandia.gov (M. Nyman).

0022-4596/$ - see front matter Published by Elsevier Inc.
doi:10.1016/S0022-4596(03)00354-2

case of the inter-slab space containing negatively charged $[AO]^-$ layers (A = alkali); electrostatic stabilization is increased by concentrating the more highly charged Nb^V near the inter-slab space [23].

While three-dimensional, layered and microporous solids featuring partially or completely disordered Ti^{IV}/Nb^VO_6 octahedra are common, cluster compounds containing Ti^{IV}/Nb^VO_6 octahedra are not, to our knowledge, known. Polyoxometalates, which are anionic clusters composed of assemblies of edge- and corner-sharing distorted octahedra of d^0 early transition metals [26], are readily formed by Nb^VO_6 octahedral building blocks but not $Ti^{IV}O_6$ octahedral building blocks. Polyoxoniobate chemistry has thus far been dominated by the Lindquist $[Nb_6O_{19}]^{8-}$ ion [27,28]. Recently, we have been investigating synthetic methods to diversify this chemistry and expand this class of materials [29]. In polyoxoniobate cluster geometries, the Nb^VO_6 octahedra are distorted with a long Nb–O bond towards the interior of the cluster, trans to a short, terminal Nb–O bond on the exterior of the cluster. There are several examples in which $Ti^{IV}O_6$ octahedra are substituted into polyoxotungstate and polyoxomolybdate clusters, but in the solid state, these $Ti^{IV}O_6$ octahedra never contain terminal Ti–O bonds. Instead, they feature terminal Ti–OH bonds [30], terminal ligands bonded to Ti^{IV} such as $C_5H_5^-$ or $C_2O_4^-$ [31–33], or Ti^{IV} located in unique cluster positions in which all oxygen of the $Ti^{IV}O_6$ octahedron are shared [34,35]. In the latter case, unprecedented polyoxometalate cluster types have been formed, presumably with the driving force to stabilize $Ti^{IV}O_6$ octahedra (often by condensation) into less-distorted positions that do not contain terminal Ti–O or Ti–OH bonds.

We present here synthesis and structural characterization of $Na_8[Nb_8Ti_2O_{28}]\cdot 34H_2O$ [1], where $[Nb_8Ti_2O_{28}]^{8-}$ is a polyoxometalate assembly that contains both $Ti^{IV}O_6$ and Nb^VO_6 octahedra within the cluster. As with the Ti^{IV}-substituted W^{VI} and Mo^{VI} polyoxometalate clusters reviewed above, the $Ti^{IV}O_6$ octahedra are located in cluster positions in which all oxygens are shared between at least two octahedra. In addition to representing the first example of a Ti^{IV}/Nb^VO_6 polyoxometalate, this cluster presents an opportunity for experimental and theoretical investigations of the stability of $Ti^{IV}O_6$ octahedra within a polyoxoniobate cluster, and conversely the stabilization effects of $Ti^{IV}O_6$ octahedra on the polyoxoniobate cluster. In addition to reporting the synthesis and characterization of [1], we present molecular mechanics calculations of the stability of the deca-titanoniobate cluster as a function of Ti^{IV} location. The purpose of these investigations is to contribute to the understanding of factors that control structure, morphology, stability and functionality of materials. By understanding these parameters, we can gain a level of prediction and thus control material formation from the atomic level.

2. Experimental

2.1. Synthesis

Amorphous niobium pentoxide (0.35 g, 2.6 mmol Nb) and titanium isopropoxide (0.25 g, 0.88 mmol) are combined in an 8 mL NaOH solution (0.34 M) in a 23 mL Teflon-lined Parr pressure vessel and stirred for approximately 20 min. The closed vessel is placed in an oven at 200–220°C for 5–20 h. The product is a mixture of white powder and large (100–500 μm diameter), irregular-shaped, colorless crystals that dehydrate quickly (become cracked and translucent) when removed from the mother liquor. To obtain a pure batch of crystals, the product mixture is stirred in de-ionized water. The crystals dissolve and the white powder is filtered off. A clear solution is obtained from this treatment that contains the dissolved crystals. Slow diffusion of methanol into the solution at room temperature produces well-formed crystals of [1]. We have obtained yields ranging from 50% to 80% (based on Nb: the Ti is in excess in the synthesis). The large range in yield is owed to the recrystallization step: the amount of product obtained from recrystallization is a function of the concentration of the solution from which [1] crystallizes, the temperature during recrystallization, and the geometry of the container in which the process takes place.

2.2. Structure determination

From the recrystallized batch of [1], a suitable crystal was selected (average diameter ~150 μm) and mounted on a glass fiber with Fluorolube (Occidental Chemical Corp., Dallas, TX, USA) in order to prevent dehydration. The intensities were measured at low temperature (−50°C) using a Bruker AXS CCD diffractometer. Data collection and reduction were carried out with the SMART [36] and SAINT-PLUS software [37] and an empirical absorption correction was done with SADABS [38].

The structure was solved by direct methods in the space-group P-1 using the program SIR-97 [39] and refined with SHELX-97 [40]. All calculations were performed using the WinGX system [41]. Anisotropic atomic displacement parameters were refined for all non-hydrogen atoms. Hydrogen atoms could be located by difference Fourier maps for 14 out of 17 independent water molecules. These hydrogen positions were refined by constraining all O–H distances to be equal within 0.02 Å, giving a total of 28 O–H distances constrained, leading to $\frac{1}{2}\times(28\times 27)=378$ least squares restraints (see Table 1). The three remaining oxygen atoms of the water molecules (O32, O33, and O34) have a displacement parameter about twice as large as those of the other water molecules, which prevented the location of

Table 1
Crystal data and structure refinement for $Na_8[Nb_8Ti_2O_{28}]\cdot 34H_2O$

Empirical formula	$Na_8[Nb_8Ti_2O_{28}]\cdot 34H_2O$
Formula weight	2083.54
Temperature	223(2) K
Wavelength	0.71073 Å
Crystal system	Triclinic
Space group	*P*-1
Unit-cell dimensions	$a = 11.829(4)$ Å, $\alpha = 97.666(5)^\circ$ $b = 12.205(4)$ Å, $\beta = 113.840(4)^\circ$ $c = 12.532(4)$ Å, $\gamma = 110.809(4)^\circ$
Volume	1463.5(8) Å^3
Z	1
Density (calculated)	2.364 g/cm^3
Absorption coefficient	1.950 mm^{-1}
F(000)	1024
Crystal size	$0.2\times 0.1\times 0.1$ mm^3
Theta range for data collection	1.89–28.05°
Index ranges	$-15\leqslant h\leqslant 15$, $-15\leqslant k\leqslant 15$, $-16\leqslant l\leqslant 16$
Reflections collected	12612
Independent reflections	6586 [R(int) = 0.0181]
Completeness to $\theta = 28.05^\circ$	92.7%
Refinement method	Full-matrix least-squares on F^2
Data/restraints/parameters	6586/378/449
Goodness-of-fit on F^2	1.042
Final R indices [$I>2\sigma(I)$]	$R_1 = 0.0241$, w$R_2 = 0.0647$
R indices (all data)	$R_1 = 0.0267$, w$R_2 = 0.0664$
Largest diff. peak and hole	2.480 and −0.704 e Å^{-3}

the hydrogen atoms. The population parameter for the water molecules and sodium atoms were initially refined and all those sites were found to be fully occupied. The refinement converged to the final agreement indices $R_1 = 0.0241$ and w$R_2 = 0.0647$ for 6086 reflections with $I>2\sigma(I)$. Crystal data and refinement details are given in Table 1.

2.3. Compositional analysis

Compositional analysis of [1] was executed on a Perkin–Elmer Sciex Elan 6100 inductively coupled plasma mass spectrometer (ICP-MS) using an argon plasma flame and dual detector mode. Standards for linear regression curves for Na, Ti and Nb (0.1, 1, 5, 10, 20 ppm) were made by appropriate dilution of 1000 ppm standards (Nb standard from SPEX; Na and Ti standards from VHG labs). A sample of [1] (18.9 mg, recrystallized and dehydrated) was dissolved in three drops of HF and diluted to 1000 mL with DI H_2O and 1 mL 6 M Nitric acid.

2.4. Molecular modeling

Energy minimizations were performed to examine the relative stability of all possible structural isomers of the deca-titanoniobate cluster, as well as the deca-niobate cluster. The crystal structure data for the deca-titanoniobate reported in this study were used for the initial model structure. The energies for each cluster were calculated using the universal force field (UFF) [42] in which the force field parameters are generated from a set of rules based on element, hybridization, and connectivity. The energy expression for this force field is

$$E_{\text{total}} = E_{\text{bond}} + E_{\text{angle}} + E_{\text{torsion}} + E_{\text{VdW}} + E_{\text{Coulomb}},$$

where E_{total} is the total energy of the system; the bonded energy terms—E_{bond}, E_{angle}, and E_{torsion}—represent the energy due to bond-stretching, angle-bending, and torsion, respectively; and, the non-bonded terms, E_{VdW} and E_{Coulomb}, are the energy contributions due to van der Waals interactions and electrostatics. The van der Waals interactions are described by a Lennard–Jones potential, which is attenuated by a spline function at an interaction cutoff distance of between 11 and 14 Å. Beyond this distance, van der Waals interactions are ignored. The Coulombic interactions are calculated using the Ewald summation method that accurately determines the energy associated with long-range electrostatic forces [43]. The unique oxygen environments in the titanoniobate cluster are not specifically defined by UFF. Therefore, we modified the oxygen type geometries to more closely approximate the observed structure of the cluster.[1] A comparison of the calculated deca-titanoniobate structure with that observed experimentally is provided in the next section. Using the charge equilibration algorithm of Rappé and Goddard [44], the charge of the cluster (−8) was redistributed over the atoms for each rearrangement of Nb and Ti polyhedra prior to energy minimization.

3. Results and discussion

3.1. Structure description

The $[Ti_2Nb_8O_{28}]^{8-}$ cluster has the same geometry as the decaniobate cluster reported by Graeber and Morosin [45]. Atomic coordinates and atomic displacement parameters for non-hydrogen atoms are summarized in Table 2, and relevant intra-cluster bond lengths and bond angles are compiled in Table 3. The decameric cluster can be described as a 2×3 rectangle of edge-sharing octahedra, capped by two edge-sharing octahedra above and below the plane of the rectangle (Fig. 1). It may also be viewed as two interpenetrating hexaniobate clusters, where each hexaniobate cluster has one octahedron removed. Fig. 2 shows the cluster as a ball-and-stick model. Each NbO_6 octahedron has a very short terminal Nb–O bond (1.759(2)–1.765(2) Å; O10,

[1] For the apical oxygens, $r_i = 0.4$ Å, $\theta_o = 180^\circ$, $Z_i = 2.998$, $V_i = 0$ kcal/mol, and $E_\omega = 0$ kcal/mol. For two- and three-fold oxygens, $r_i = 0.528$ Å, $\theta_o = 109^\circ$, $Z_i = 2.998$, $V_i = 0.018$ kcal/mol, and $E_\omega = 0$ kcal/mol. For six-fold oxygens, $r_i = 1.4$ Å, $\theta_o = 90^\circ$, $Z_i = 4.000$, $V_i = 0.0$, and $E_\omega = 12.0$ kcal/mol. For equations and definitions, see Ref. [42].

Table 2
Atomic coordinates and atomic displacement parameters for non-hydrogen atoms for $Na_8[Nb_8Ti_2O_{28}] \cdot 34H_2O$

Atom	Specie	X	Y	Z	U_{eq}[a]
Nb1	Nb	0.08981(2)	0.11504(2)	0.31858(2)	0.01185(6)
Nb2	Nb	−0.27482(2)	0.80540(2)	0.82521(2)	0.01140(6)
Nb3	Nb	−0.20730(2)	0.01559(2)	0.05922(2)	0.01140(6)
Nb4	Nb	−0.04208(2)	0.69945(2)	0.85854(2)	0.01214(6)
Ti1	Ti	0.02344(4)	0.91099(4)	0.08601(4)	0.00987(9)
O1	O	−0.17961(17)	0.85742(15)	0.01826(15)	0.01155(32)
O2	O	0.02921(17)	0.09064(15)	0.10131(15)	0.01196(33)
O3	O	0.08598(18)	0.27198(16)	0.30182(16)	0.01454(34)
O4	O	0.21540(17)	0.00411(15)	0.11346(15)	0.01211(33)
O5	O	−0.04806(20)	0.55122(17)	0.83717(18)	0.01961(38)
O6	O	0.00850(18)	0.75639(16)	0.03801(16)	0.01389(34)
O7	O	0.27220(18)	0.17908(16)	0.32442(16)	0.01480(34)
O8	O	−0.23399(18)	0.66594(16)	0.82117(16)	0.01476(34)
O9	O	−0.11551(18)	0.03539(16)	0.23202(16)	0.01439(34)
O10	O	0.13605(20)	0.12860(18)	0.47416(17)	0.01952(38)
O11	O	−0.45152(18)	0.74436(17)	0.78397(17)	0.01859(37)
O12	O	0.06836(18)	0.94466(16)	0.24750(16)	0.01369(34)
O13	O	−0.38162(18)	0.95268(17)	0.02477(17)	0.01900(39)
O14	O	0.15586(18)	0.81093(16)	0.91628(16)	0.01445(34)
O20	Ow[b]	0.61987(23)	0.12781(22)	0.21191(21)	0.02739(45)
O21	Ow	0.30576(22)	0.11366(22)	0.69975(20)	0.02830(47)
O22	Ow	−0.01930(23)	0.80140(20)	0.39001(21)	0.02483(43)
O23	Ow	0.55129(23)	0.02333(21)	0.70987(20)	0.02498(43)
O24	Ow	0.48607(24)	0.19590(24)	0.54531(21)	0.03071(49)
O25	Ow	0.69067(26)	0.69635(21)	0.12499(22)	0.02977(48)
O26	Ow	0.60495(22)	0.22440(20)	0.96622(20)	0.02312(41)
O27	Ow	−0.01193(27)	0.53858(22)	0.34334(22)	0.03143(49)
O28	Ow	0.33403(25)	0.68088(23)	0.54227(22)	0.03271(51)
O29	Ow	0.25650(22)	0.86193(22)	0.39079(21)	0.02626(44)
O30	Ow	0.10678(24)	0.69801(21)	0.63824(20)	0.02696(44)
O31	Ow	−0.15727(28)	0.54834(24)	0.07415(25)	0.03650(55)
O32	Ow	0.36537(34)	0.47502(27)	0.46838(29)	0.06088(81)
O33	Ow	0.58468(35)	0.44064(26)	0.83097(27)	0.06537(96)
O34	Ow	0.30842(36)	0.38063(28)	0.63634(33)	0.06923(99)
O35	Ow	0.61083(25)	0.40867(20)	0.13186(23)	0.03061(49)
O36	Ow	0.78707(23)	0.30837(21)	0.81314(22)	0.02821(47)
Na1	Na	0.15257(12)	0.73517(11)	0.48317(11)	0.02731(25)
Na2	Na	0.54898(12)	0.22340(11)	0.75943(11)	0.02539(24)
Na3	Na	−0.19219(12)	0.59594(11)	0.24967(11)	0.02741(25)
Na4	Na	0.5	0	0.5	0.02508(33)
Na5	Na	0.5	0.5	0	0.12888(201)

[a] U_{eq} is defined as 1/3 of the trace of the orthogonalized U_{ij} tensor.
[b] Ow is a water molecule.

O11, O13, O5) on the exterior of the cluster. Trans to the short Nb–O bond is a long Nb–O bond (2.409(2)–2.481(2) Å) to O2, and O2 bridges six octahedra. The remaining four equatorial Nb–O bonds range from 1.921(2) to 2.104(2) Å, and the oxygen atoms are bridging two or three octahedra. The doubly bridging oxygen atoms (O3, O6, O7, O8, O9, O12, O14) have Nb–O bond lengths from 1.921(2) to 2.032(2) Å, and the triply bridging oxygen atoms (O1, O4) have slightly longer Nb–O bond lengths, all around 2.1 Å (2.099(2)–2.104(2)). The triply bridging oxygen atoms bridge two NbO_6 octahedra and one TiO_6 octahedra each, and the doubly bridging oxygen atoms bridge two NbO_6 octahedra or one TiO_6 and one NbO_6 octahedra. The Ti atoms are located in the octahedral positions of the cluster that have no terminal oxygen bonds. Each Ti atom is bonded to two octahedral oxygen atoms (O2), two triply bridging oxygen atoms (O1 and O4), and two doubly bridging oxygen atoms (O6 and O12). The Ti–O bonds to the three-coordinate oxygen atoms are 1.999(2) and 2.001(2) Å, the Ti–O bonds to the octahedral oxygen atoms are 2.150(2) and 2.167(2) Å, and the Ti–O bonds to the two-coordinate oxygen atoms are 1.817(2) and 1.824(2) Å. In general, the Ti–O bond lengths are dictated by the coordination geometries of the oxygen atoms: the Ti–O bond length increases with increasing number of bonds to the coordinated oxygen atom.

An overall view of the structure is shown in Fig. 3. Between the $[Nb_8Ti_2O_{28}]^{8-}$ clusters are water molecules and charge-balancing Na atoms. All Na sites are fully occupied. Na1, Na2, and Na3 have multiplicities of 2. Na4 and Na5, which are located on special symmetry positions, have multiplicities of 1 each. Overall, this gives eight Na atoms per cluster, which results in a charge-balanced structure. There are 17 water molecule sites, each with a multiplicity of two, giving 34 water molecules per cluster. Each sodium atom is bonded to five or six water molecules with Na-Ow bond lengths ranging from 2.277(3)–2.799(3) Å with an average of 2.436 Å. The Na–Ow network forms "chains" that run parallel to (011). The hydrogen atoms were located for all water molecules except O32, O33, and O34. Hydrogen bonding is weak to moderate, both between two water molecules and between a water molecule and a cluster oxygen. The closest $H–O_{cluster}$ distance observed is around 2.0 Å, the closest H–Ow (non-bonded) distance is around 2.0 Å, and the closest $Ow–O_{cluster}$ distance is around 2.8 Å. Neither the terminal nor bridging oxygen atoms of the cluster bond with the Na atoms. The closest $Na–O_{cluster}$ distance is around 4 Å. This lack of interaction between the clusters and the Na–water network explains why these crystals easily dissolve in water, and readily dehydrate upon exposure to air.

3.2. Other characterizations of [1]

The ICP-MS results of the solution of previously dehydrated [1] gave 8.25 ppm Nb, 1.06 ppm Ti and 2.00 ppm Na, which translates to a chemical formula of $Nb_{8.02}Ti_2Na_{7.86}$ (normalized to Ti) that is in excellent agreement with the formula defined by the single-crystal X-ray analysis. Dehydration of [1] does not change the metal ratios. This confirms that the composition found by single-crystal X-ray diffraction agrees with the composition of the bulk sample. Additionally, the good agreement of the compositional analysis with the single-crystal X-ray data indicates sample purity.

The dehydrating nature of the crystals presented many challenges in terms of bulk characterization of [1].

Table 3
Selected bond angles (deg) and bond distances (Å) within the $[Nb_8Ti_2O_{28}]^{8-}$ cluster

Atom	$O(x)_1$	A–$O(x)_1$ bond length (Å) (e.s.d.)	$O(x)_2$	$O(x)_1$–A–$O(x)_2$ bond angle (deg) (e.s.d.)	Atom	$O(x)_1$	A–$O(x)_1$ bond length (Å) (e.s.d.)	$O(x)_2$	$O(x)_1$–A–$O(x)_2$ bond angle (deg) (e.s.d.)
Nb1	O2	2.4638(19)	O9	77.03(6)	Nb2	O1	2.0986(18)	O11	101.61(8)
	O7	1.9823(19)	O3	88.29(7)		O2	2.4094(18)	O7	79.06(7)
	O9	1.9829(19)	O3	87.99(7)		O4	2.1013(18)	O7	89.53(7)
	O10	1.7651(19)	O3	104.98(8)		O7	1.9211(18)	O11	104.34(8)
	O12	2.0323(18)	O9	85.44(7)		O8	1.9271(18)	O7	94.40(8)
	O3	1.9689(18)	O2	76.97(6)		O11	1.7631(19)	O4	100.16(8)
	O2		O7	76.61(6)		O1		O4	74.40(7)
	O2		O12	74.45(6)		O2		O4	73.91(6)
	O7		O10	102.34(8)		O2		O1	73.99(6)
	O7		O12	85.39(7)		O1		O8	89.76(7)
	O9		O10	103.92(8)		O2		O8	79.66(7)
	O10		O12	103.60(8)		O8		O11	105.63(8)
Nb3	O1	2.1019(18)	O9	89.91(7)	Nb4	O6	2.0246(19)	O14	85.33(7)
	O4	2.1041(18)	O1	74.27(6)		O2	2.4813(19)	O3	76.44(6)
	O13	1.7592(18)	O1	102.98(8)		O3	1.9753(18)	O5	106.11(8)
	O9	1.9235(18)	O13	101.19(8)		O5	1.7647(19)	O8	103.66(8)
	O14	1.9256(19)	O2	79.59(6)		O8	1.9924(19)	O3	87.77(7)
	O2	2.4087(18)	O1	73.97(6)		O14	1.9903(19)	O2	76.62(6)
	O13		O14	103.32(8)		O8		O2	74.46(6)
	O4		O13	104.73(8)		O14		O5	102.91(8)
	O1		O9	89.91(7)		O2		O8	76.70(6)
	O14		O9	94.97(8)		O6		O5	102.99(8)
	O14		O4	89.18(7)		O6		O8	85.81(7)
	O9		O2	79.48(7)		O3		O14	87.81(7)
Ti1	O1	2.0013(18)	O2	81.97(7)	Ti1	O4		O6	96.37(8)
	O4	1.9992(18)	O12	96.85(8)		O1		O12	96.62(7)
	O2	2.1495(18)	O4	81.95(7)		O1		O6	96.18(8)
	O6	1.8242(18)	O12	105.55(8)		O1		O2′	81.50(7)
	O2’	2.1669(18)	O2	80.74(7)		O4		O2′	81.76(7)
	O12	1.8167(18)	O2	87.03(7)		O6		O2′	86.67(7)

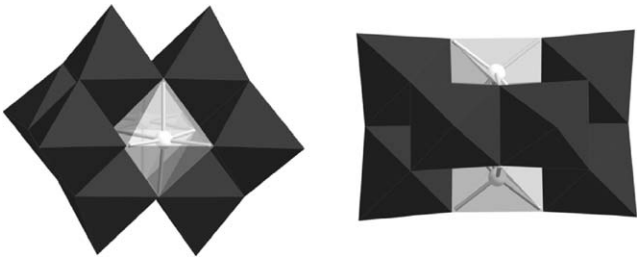

Fig. 1. Two views of $[Nb_8Ti_2O_{28}]^{8-}$. The dark, opaque octahedra are NbO_6 and the transparent octahedra are TiO_6.

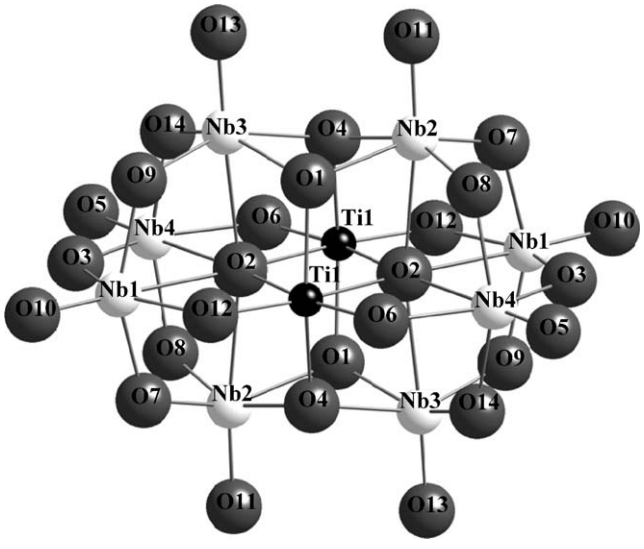

Fig. 2. A ball-and-stick model of $[Nb_8Ti_2O_{28}]^{8-}$.

Optical observation of the crystals reveals that they become cracked and opaque within minutes upon removal from the mother liquor. The crystals that are obtained directly from the mother liquor and those that are recrystallized are equally susceptible to dehydration. As expected, the powder diffraction pattern of dehydrated crystals of [1] does not match the pattern calculated from the structure obtained from the single-crystal data of hydrated [1]. The powder diffraction pattern shows that the dehydrated [1] is still well crystallized, and thus dehydration does not result in decomposition and amorphization. Further structural characterization of dehydrated [1] is beyond the scope of

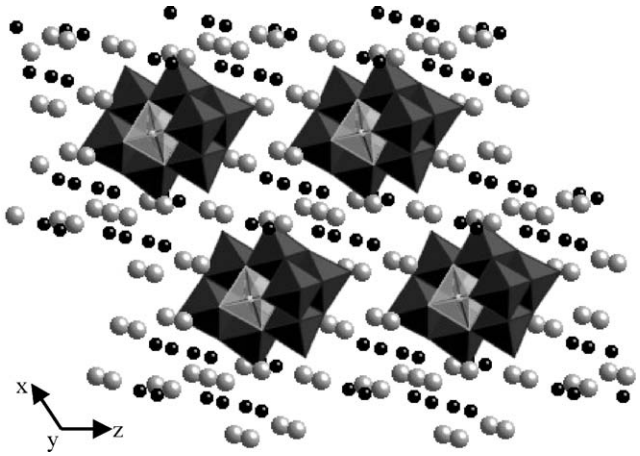

Fig. 3. An overall view of $Na_8[Nb_8Ti_2O_{28}]\cdot 34H_2O$ [1], down the *y*-axis. The dark, opaque octahedra are NbO_6 and the transparent octahedra are TiO_6, and the light spheres are Na^+. The dark spheres are oxygen of the water molecules. The hydrogen atoms are omitted for clarity.

this study. The single crystal was indeed measured under protective oil and at low temperature (223 K) in order to prevent dehydration. Complete structure determination was in fact carried out on two different crystals: the first crystal was taken directly from the mother liquor, and the second crystal (of higher quality) was from a batch that was removed from the mother liquor (and thus dehydrated), redissolved and recrystallized. Both data sets yielded the same structure within experimental errors, strongly suggesting stability of the anionic cluster, both upon dehydration and recrystallization.

3.3. Synthetic investigations of $[Nb_8Ti_2O_{28}]^{8-}$ stability

Graeber and Morosin [45] in 1977 synthesized a $[Nb_{10}O_{28}]^{6-}$ cluster with the same geometry as [1]. They obtained this deca-cluster in two different compounds: one with tetramethylammonium as the charge-balancing cations, and the second with a mixture of sodium and tetramethylammonium as the charge-balancing cations. They reported similar physical characteristics as the crystals of [1], in the tendency of the crystals to dehydrate. Since this current study focuses on the stabilization effect of the TiO_6 octahedra on the cluster geometry (by both experimental and theoretical approaches), we carried out synthetic investigations into the formation and stability of the decaniobate, $[Nb_{10}O_{28}]^{6-}$. For both compounds reported by Graeber and Morosin, hydrolysis of niobium ethoxide dissolved in methanol solution was the method from which they obtained the niobium-oxo clusters. We attempted this synthetic method to obtain $[Nb_8Ti_2O_{28}]^{8-}$; with sodium as the counterion and with tetramethylammonium as the counterion, using the appropriate mixture of titanium isopropoxide and niobium ethoxide. Conversely, we attempted to produce $[Nb_{10}O_{28}]^{6-}$ using the general hydrothermal synthetic method from which we obtained [1]. From these synthetic experiments, we found that: (1) we could not form $[Nb_8Ti_2O_{28}]^{8-}$ nor $[Nb_{10}O_{28}]^{6-}$ using the method reported by Graeber and Morosin, and (2) we obtained hexaniobate, $[Nb_6O_{19}]^{8-}$, from the hydrothermal synthesis method, when titanium was not included in the reaction.

From these results, we have concluded that: (1) In the absence of heteroatoms such as titanium, $[Nb_6O_{19}]^{8-}$ is the dominant specie of basic, aqueous solutions of niobium oxide. (2) Formation of metal–oxo clusters by partial hydrolysis and condensation of moisture- and air-sensitive metal alkoxides is heavily influenced by the initial state of the alkoxide precursor. These conclusions are discussed further, below.

The literature on niobium oxide aqueous chemistry gives much evidence for the Lindquist ion as the dominant Nb–O specie in basic aqueous solutions. Several works give experimental evidence that $[Nb_6O_{19}]^{8-}$ is the dominant Nb–O specie in basic solutions, while $[Nb_{10}O_{28}]^{6-}$ is not a commonly observed specie in aqueous solution [46,47]. Further, $[Nb_6O_{19}]^{8-}$ has been formed using a number of synthetic methods and with various counterions [28,48]. Additionally, $[Nb_6O_{19}]^{8-}$ has been used as coordinating "ligands" for heterometals [49–51], which suggests its robustness in a variety of processing conditions upon dissolution and reprecipitation. Finally, few polyoxoniobate geometries other than the Lindquist ion have been produced [29].

Since $[V_{10}O_{28}]^{6-}$, isostructural to $[Nb_{10}O_{28}]^{6-}$, is a common V–O specie both in the solid state and in solution [52,53], the formation of $[Nb_{10}O_{28}]^{6-}$ is not absolutely unexpected. However, the rarity of evidence for the existence of $[Nb_{10}O_{28}]^{6-}$ in the solid state or in solution suggests it is a rather unstable cluster geometry. Our experiments described above suggest that the Graeber and Morosin reaction is inherently irreproducible, given the unstable nature of niobium alkoxides when handled in ambient conditions.[2] Rather than representing a stable, anionic metal–oxo specie in solution, the $[Nb_{10}O_{28}]^{6-}$ produced by Graeber and Morosin more likely represents a pre-hydrolyzed state of the niobium alkoxide precursor, in that metal alkoxides including niobium alkoxide [54–56] are known to form metal–oxo–alkoxy clusters as intermediates to final hydrolysis and condensation products.

In contrast, the $[Nb_8Ti_2O_{28}]^{8-}$ synthesis reported here can be reproduced readily and in aqueous conditions that warrant complete hydrolysis and condensation of

[2] Discussion with B. Morosin, investigations into archived lab notebooks revealed that the decaniobate clusters were made without the aid of an inert atmosphere boxes or special handling of the niobium alkoxide precursor.

metal (titanium) alkoxide precursors. Further, the fact that [1] could be recrystallized from solution is strong evidence that it is a stable anion in aqueous solution. This suggests the titanium in the central octahedral positions stabilizes the deca-cluster geometry, and addition of a heteroatom such as titanium is a reliable method to predictably and reproducibly form this geometry, or some other geometry that could not be obtained otherwise.

3.4. Calculated structures and energetics of $[Nb_8Ti_2O_{28}]^{8-}$ isomers

The calculated structures of all the possible isomers of $[Nb_8Ti_2O_{28}]^{8-}$ are shown in Fig. 4. A comparison of pertinent bond angles and bond lengths of the calculated and structurally determined geometry of [1] are shown in Table 4. In general, there is a good agreement between the calculated and experimental structures, in the case of the isomer observed in [1]. The major deviation is in the O2–Ti–O2′ bond angle; this angle is 16° larger in the calculated structure, which brings the two Ti atoms closer together. This also moves the O2 and O2′ positions out from the center of the cluster, and results in slightly shorter Nb–O interior bonds and slightly longer Nb–O exterior bonds (i.e. slightly less distorted NbO_6 octahedra). In fact, it appears the interior M–O2(2′) (M = Nb, Ti) bond length is a direct reflection of cluster stability of the calculated isomers, and is discussed below.

We have identified an approximate correlation of cluster energy with the average M–O2(2′) bond lengths (M = Ti, Nb) in each cluster, where O2 and O2′ are the hexacoordinate oxygen atoms within the cluster. This relationship of decreasing stability with increasing M–O2(2′) bond distances is seen in Table 5. Also illustrated in Table 5 is cluster stability as a function of number of edges shared by TiO_6 and NbO_6 octahedra within the cluster, respectively. As shown in Fig. 5, seven MO_6 edges are shared for octahedra type A, five MO_6 edges are shared for octahedra type B and four MO_6 edges are shared for octahedra of type C (M = Ti, Nb). These observed trends may be summarized by the following generalizations: (1) stability is increased with increased

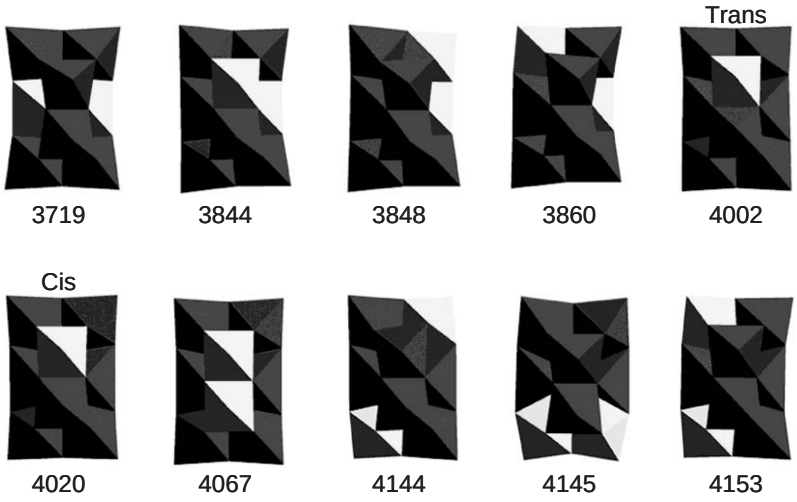

Fig. 4. The 10 possible isomers of $[Nb_8Ti_2O_{28}]^{8-}$ and their calculated cluster energies in units kilocalories per cluster. Increasing energy corresponds with decreasing stability. The clusters labeled "*cis*" and "*trans*" have the second TiO_6 octahedron in the position, respectively, *cis* and *trans* to the TiO_6 octahedron observable in the observed orientation.

Table 4
Comparison of energies and structural parameters of calculated and X-ray determined structures of $[Nb_8Ti_2O_{28}]^{8-}$ and $[Nb_{10}O_{28}]^{6-}$

Bond length (Å) or bond angle (deg)	Calculated structure		Structure determined from X-ray data	
	$[Nb_8Ti_2O_{28}]^{8-}$	$[Nb_{10}O_{28}]^{6-}$	$[Nb_8Ti_2O_{28}]^{8-}$	$[Nb_{10}O_{28}]^{6-}$
Short axial (exterior) Nb–O (Å)	1.80	1.80	1.76	1.74
Long axial (interior) Nb–O (Å)	2.32–2.38	2.38–2.53	2.41–2.48	2.41–2.55
Equatorial Nb–O (Å)	1.97–2.00	1.93–1.97	1.92–2.10	1.91–2.10
Ti–O (all) (Å)	1.89–2.23	N/A	1.82–2.15	N/A
O2–M_A[a]–O2′ (M = Ti, Nb) (deg)	96.3	64.7	80.8	76.9
Calculated energies (kcal/cluster)	3719	4434		

[a] M_A is the metal in the A-type octahedron.

Table 5
Calculated energies and related parameters of $[Nb_8Ti_2O_{28}]^{8-}$ polymorphs

Cluster polymorph described by TiO_6 octahedral positions[a]	Calculated energy of cluster (kcal/cluster)	Average M–O2[b] bond distance, Å (M = Ti, Nb)	Number of edges shared by TiO_6 octahedra	Number of edges shared by NbO_6 octahedra
A, A (observed)	3719	2.30	14	36
A, C	3844	2.33	11	39
A, C	3848	2.34	11	39
A, B	3860	2.33	12	38
B, B	4002	2.40	10	40
B, B	4020	2.40	10	40
B, B	4067	2.40	10	40
C, C	4144	2.42	8	42
C, C	4145	2.43	8	42
C, C	4153	2.65	8	42

[a] Octahedron A shares seven cluster edges, octahedron B shares five cluster edges, octahedron C shares four cluster edges (see Fig. 5).
[b] The M–O2 bond is the long, axial bond of the distorted octahedra.

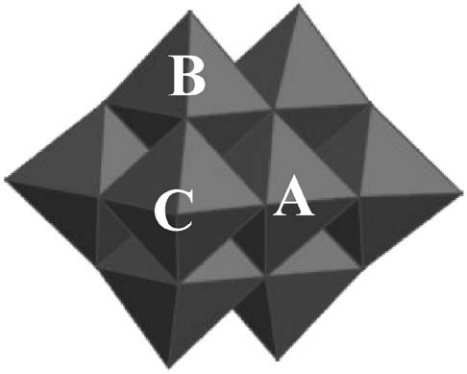

Fig. 5. The three cluster types that make up $[M_{10}O_{28}]$ based on number of MO_6 edges shared within the cluster (M = Ti, Nb): cluster type A shares seven edges within the cluster, cluster type B shares five edges within the cluster and cluster type C shares four edges within the cluster.

TiO_6 edge-sharing within the cluster, (2) stability is decreased with increased NbO_6 edge-sharing within the cluster, and (3) there is increased repulsion between cluster octahedra with increased NbO_6 edge-sharing and decreased TiO_6 edge-sharing, as reflected in increasing M–O2(2′) bond distance with decreasing cluster stability. Finally, one of Pauling's rules summarizes these observations as: increased repulsion between edge-sharing polyhedra results from increased metal cation size and charge. Since Nb^{5+} has both a larger size and radius than Ti^{4+}, repulsion is greater between edge-sharing NbO_6 than between edge-sharing TiO_6. In general, this suggests that the origin of distortion in NbO_6 octahedra is to minimize repulsion between edge-sharing octahedra in extended solids or clusters.

3.5. Comparison of structures and energetics of $[Nb_8Ti_2O_{28}]^{8-}$ and $[Nb_{10}O_{28}]^{6-}$

Some pertinent bond angles and bond lengths of $[Nb_8Ti_2O_{28}]^{8-}$ and $[Nb_{10}O_{28}]^{6-}$ are compared in Table 4. In general, the X-ray determined structures of these clusters are very similar. Notable differences include a slightly smaller O2–M_A–O2′ bond angle for $[Nb_{10}O_{28}]^{6-}$, where M_A is the metal in the A-type octahedra position (Ti in the case of $[Nb_8Ti_2O_{28}]^{8-}$; Nb in the case of $[Nb_{10}O_{28}]^{6-}$). Also, $[Nb_{10}O_{28}]^{6-}$ has slightly longer interior Nb–O bond lengths, including one at 2.55 Å, where 2.54 Å is considered the maximum Nb–O bond length, according to radii compiled by Shannon and Prewitt (Shannon, 1970 #59). This difference is exaggerated in the calculated structures: in the X-ray determined structures there is an approximate 4° difference between the O2–M–O2′ angles of the two deca-clusters and in the calculated structures there is ~30° difference between this angle of these two clusters. According to the energy calculations, the $[Nb_8Ti_2O_{28}]^{8-}$ cluster is more stable than the $[Nb_{10}O_{28}]^{6-}$ cluster by about 700 kcal/cluster (Table 4). As we learned from the theoretical investigations of the $[Nb_8Ti_2O_{28}]^{8-}$ isomers, the structural differences (both calculated and experimentally determined) between these clusters likely result from greater repulsion between the A-type octahedra containing Nb^{5+} compared to those with Ti^{4+}.

4. Summary

From our exploratory synthesis investigations in determining methods of forming new polyoxoniobate clusters, we have produced $Na_8[Nb_8Ti_2O_{28}]\cdot 34H_2O$ [1]. Molecular modeling studies of the theoretical isomers of $[Nb_8Ti_2O_{28}]^{8-}$ suggest that the smaller charge and radius of Ti^{4+} compared to Nb^{5+} stabilizes this cluster geometry by decreasing the overall repulsion between edge-sharing octahedra within the cluster. Without the titanium in the synthesis solution, the hexaniobate Lindquist ion is the preferred cluster geometry. However, with the added titanium, the decacluster becomes stable. Further, the fact that [1] can be recrystallized

from solution strongly suggests it is stable in solution as well as the solid state. In general, we have learned from this combined synthetic and molecular modeling study that addition of heteroatoms may be used as a synthetic strategy to stabilize heteropolyanion and isopolyanion geometries that may not be obtained otherwise.

Acknowledgments

This research was partially supported by the Laboratory Directed Research and Development Program at Sandia National Laboratories. Sandia is a multiprogram laboratory operated by Sandia Corporation, a Lockheed Martin company, for the United States Department of Energy under contract DE-AC04-94AL85000.

We thank Dr. Bruno Morosin for enlightening and informative historical perspective regarding his work on the $[Nb_{10}O_{28}]^{6-}$ cluster.

References

[1] A.V. Voloshin, V.V. Subbotin, Y.A. Pakhomovskii, A.Y. Bakhchisaraitsev, N.A. Yamnova, D.Y. Pushcharovskii, Dokl. Akad. Nauk SSR 315 (1990) 1218.
[2] V.V. Subbotin, A.V. Voloshin, Y.A. Pakhomovskii, A.Y. Bakhchisaraitsev, D.Y. Pushcharovskii, R.K. Rastsvetaeva, T.N. Nadezhina, Dokl. Akad. Nauk SSR 358 (1998) 517.
[3] A.R. Chakhmouradian, R.H. Mitchell, Can. Mineral. 35 (1997) 1293.
[4] L.N. Kogarko, C.T. Williams, A.R. Woolley, Mineral. Petrol. 74 (2002) 1.
[5] G. Ferraris, E. Belluso, A. Gula, S.V. Soboleva, O.A. Ageeva, B.E. Borutskii, Can. Mineral. 39 (2001) 1665.
[6] S.H. Byeon, H.J. Nam, Chem. Mater. 12 (2000) 1771.
[7] B. Raveau, Rev. Chim. Miner. 21 (1984) 391.
[8] H. Izawa, S. Kikkawa, M. Koizumi, Polyhedron 2 (1983) 741.
[9] M. Fang, C.H. Kim, G.B. Saupe, H.N. Kim, C.C. Waraksa, T. Miwa, A. Fujishima, T.E. Mallouk, Chem. Mater. 11 (1999) 1526.
[10] A.D. Wadsley, Acta Crystallogr. 17 (1964) 623.
[11] H. Rebbah, G. Desgardin, B. Raveau, J. Solid State Chem. 31 (1980) 321.
[12] H. Rebbah, J. Pannetier, B. Raveau, J. Solid State Chem. 41 (1982) 57.
[13] G. Svensson, L. Eriksson, Acta Crystallogr. C 55 (1999) 17.
[14] L.A. Bendersky, I. Levin, R.S. Roth, A.J. Shapiro, J. Solid State Chem. 160 (2001) 257.
[15] T.A. Kodenkandath, A.S. Kumbhar, W.L. Zhou, J.B. Wiley, Inorg. Chem. 40 (2001) 710.
[16] N.S.P. Bhuvanesh, M.P. Crosnier-Lopez, H. Duroy, J.L. Fourquet, J. Mater. Chem. 9 (1999) 3093.
[17] R.G. Anthony, R.G. Dosch, C.V. Phillip, US Patent # 6,110,378: Method of Using Novel Silico-titanates. Sandia National Laboratories, August, 2000.
[18] M. Nyman, A. Tripathi, J.B. Parise, R.S. Maxwell, T.M. Nenoff, J. Am. Chem. Soc. 124 (2002) 1704.
[19] M. Nyman, A. Tripathi, J.B. Parise, R.S. Maxwell, W.T.A. Harrison, T.M. Nenoff, J. Am. Chem. Soc. 123 (2001) 1529.
[20] A.R. Drews, W. Wong-Ng, R.S. Roth, T.A. Vanderah, Mater. Res. Bull. 31 (1996) 153.
[21] A.R. Drews, W. Wong-Ng, T.A. Vanderah, R.S. Roth, J. Alloys Compd. 255 (1997) 243.
[22] N.S.P. Bhuvanesh, M.P. Crosnier-Lopez, H. Duroy, J.L. Fourquet, J. Mater. Chem. 9 (1999) 3093.
[23] Y.S. Hong, S.J. Kim, S.J. Kim, J.H. Choy, J. Mater. Chem. 10 (2000) 1209.
[24] J. Gopalakrishnan, S. Uma, V. Bhat, Chem. Mater. 5 (1993) 132.
[25] M. Kuntz, I.D. Brown, J. Solid State Chem. 115 (1995) 395.
[26] M.T. Pope, Heteropoly and Isopoly Oxometalates, Springer, Berlin, 1983.
[27] I. Lindqvist, Arkiv. Kemi. 5 (1953) 247.
[28] A. Goiffon, E. Philippot, M. Maurin, Rev. Chim. Miner. 17 (1980) 466.
[29] M. Nyman, F. Bonhomme, T.M. Alam, M.A. Rodriguez, B.R. Cherry, J.L. Krumhansl, T.M. Nenoff, A.M. Sattler, Science 297 (2002) 996.
[30] T. Ozeki, T. Yamase, Acta Crystallogr. C47 (1991) 693.
[31] N.J. Crano, R.C. Chambers, V.M. Lynch, M.A. Fox, J. Mol. Catal. A 114 (1996) 65.
[32] J.F.W. Keana, M.D. Ogan, J. Am. Chem. Soc. 108 (1986) 7951.
[33] R.K.C. Ho, W.G. Klemperer, J. Am. Chem. Soc. 100 (1978) 6772.
[34] O.A. Kholdeeva, G.M. Maksimov, R.I. Maksimovskaya, L.A. Kovaleva, M.A. Fedotov, V.A. Grigoriev, C.L. Hill, Inorg. Chem. 39 (2000) 3828.
[35] Y. Lin, T.J.R. Weakley, B. Rapko, R.G. Finke, Inorg. Chem. 32 (1993) 5095.
[36] SMART, Bruker Analytical X-ray Systems Inc., Madison, WI, 1999.
[37] SAINT-PLUS, Bruker Analytical X-ray Systems Inc., Madison, WI, 1998.
[38] SADABS, Bruker Analytical X-ray Systems Inc., Madison, WI, 1998.
[39] A. Altomare, M.C. Burla, M. Camalli, G.L. Cascarano, C. Giacovazzo, A. Guagliardi, A.G.G. Moliterni, G. Polidori, R. Spagna, J. Appl. Crystallogr. 32 (1999) 115.
[40] SHELX97, Programs for Crystal Structure Analysis (Release 97-2), Göttingen, Germany, 1998.
[41] L.J. Farrugia, J. Appl. Crystallogr. 32 (1999) 837.
[42] A.K. Rappé, C.J. Casewit, K.S. Colwell, W.A. Goddard, W.M. Skiff, J. Am. Chem. Soc. 114 (1992) 10024.
[43] N. Karasawa, W.A. Goddard, J. Phys. Chem. 93 (1989) 7320.
[44] A.K. Rappé, W.A. Goddard, J. Phys. Chem. 95 (1991) 3358.
[45] E.J. Graeber, B. Morosin, Acta Crystallogr. B-Struct. Sci. 33 (1977) 2137.
[46] G.M. Rozantsev, O.I. Dotsenko, G.V. Taradina, Russ. J. Coord. Chem. 26 (2000) 247.
[47] G. Neumann, Acta Chem. Scand. 14 (1964) 278.
[48] R.S. Tobias, Can. J. Chem. 43 (1965) 1222.
[49] C.M. Flynn, G.D. Stucky, Inorg. Chem. 8 (1969) 335.
[50] M.F.P. Silva, A.M.V. Cavaleiro, J.D.P. DeJesus, J. Coord. Chem. 50 (2000) 141.
[51] A.V. Besserguenev, M.H. Dickman, M.T. Pope, Inorg. Chem. 40 (2001) 2582.
[52] V.W. Day, W.G. Klemperer, D.J. Maltbie, J. Am. Chem. Soc. 109 (1987) 2991.
[53] H.T. Evans, Heteropoly and isopoly complexes of the transition elements of groups 5 and 6, in: J.D. Dunitz, J.A. Ibers (Eds.), Perspectives in Structural Chemistry, Wiley, New York, 1971.
[54] R. Papiernik, L.G. Hubert-Pfaltzgraf, J.C. Daran, Y. Jeannin, J. Chem. Soc. Chem. Comm. 9 (1990) 695.
[55] N. Brinicevic, F. Mustovic, R.E. McCarley, Inorg. Chem. 27 (1988) 4532.
[56] S.K. Park, S.M. Koo, Bull. Korean Chem. Soc. 20 (1999) 1115.